[12] W. Baier, "Waves and evanescent fields in rectangular waveguides filled with a transversely inhomogenous dielectric," *IEEE Trans. Microwave Theory Tech.*, vol. MTT-18, Oct. 1970.
[13] S. Nauman and J. S. Sethares, "Design of microwave dielectric resonators," *IEEE Trans. Microwave Theory Tech.*, vol. MTT-14, pp. 2–7, Jan. 1966.
[14] E. A. Benson, *Millimeter and Submillimeter Waves*. London: Iliffe Books Ltd., 1969.
[15] E. L. Kollberg, "On measurements of noise in low-noise receiving systems," *IEEE Trans. Instrumentation and Measurements*, vol. IM-23, pp. 226–232, Sept. 1974.
[16] G. L. Matthaei, L. Young, and E. M. T. Jones, *Microwave Filters, Impedance-Matching Networks, and Coupling Structures*. New York: McGraw-Hill, 1964.
[17] E. L. Hentley, "Superconducting magnet for an 8 mm travelling-wave maser," *Cryogenics*, vol. 7, pp. 33–35, Feb. 1967.

A Traveling-Wave Maser Amplifier for 85–90 GHz Using a Slot-Fed Image-Guide Slow-Wave Circuit

APOSTLE G. CARDIASMENOS, MEMBER, IEEE, JAMES F. SHANLEY, MEMBER, IEEE, AND K. SIGFRID YNGVESSON, MEMBER, IEEE

Abstract—**A description is given of a newly developed traveling-wave maser amplifier for use at the new 13.7-m millimeter-wave radio telescope of the Five College Radio Astronomy Observatory (FCRAO) near Amherst, MA. The maser amplifier, using iron-doped rutile as the active maser material, has achieved 15-dB electronic gain in the prototype over an instantaneous bandwidth of 140 MHz in the frequency range from 85 to 90 GHz. The use of a slot-fed image-guide mode which provides a wide-bandwidth coupling to the maser material is described and analyzed. Reduction of the total system noise temperature to less than 100 K including the atmosphere can be realized with these maser devices providing an order of magnitude improvement in system sensitivity.**

I. Introduction

In the past several years, interest among radioastronomy researchers to detect rotational transitions of polyatomic molecules in interstellar space has spurred development of low-noise millimeter-wavelength receiver systems. This paper describes the prototype design of a series of millimeter-wave maser amplifiers utilizing iron-doped rutile (Fe^{3+}–TiO_2) as the active maser material. These amplifiers will allow total system noise temperatures in the range 70–120 GHz, to approach the atmospheric noise limit. The initial maser developed for the frequency range 85–90 GHz will enable reduction of the total system noise temperature including the atmosphere to less than 100 K SSB. This should be compared to the 600–800 K SSB system temperatures achieved by the present lowest noise systems which use Schottky-barrier diode mixers.

Previous masers in this frequency range have all been single-port reflection cavity devices [1]–[4]. Cavity masers are limited to a fairly narrow instantaneous bandwidth and are also, along with other reflection-type negative resistance amplifiers, not sufficiently stable at gains above about 15 dB. These amplifiers also require the development of low-noise cooled circulators operable at millimeter wavelengths. Typical cavity maser bandwidths of less than 20 MHz may be expected in this frequency range, while interstellar molecular spectral lines many times have linewidths exceeding 50 MHz. The instantaneous bandwidth of a traveling-wave maser, however, can be approximated by the relation [5]

$$\Delta f = \Delta f_L \left[\frac{3}{G_{\mathrm{dB}}{}^{e} - 3}\right]^{1/2} \tag{1}$$

where Δf_L is the intrinsic paramagnetic absorption linewidth, and $G_{\mathrm{dB}}{}^{e}$ is the midband maser electronic gain. For a typical electronic gain of 30 dB, and $\Delta f_L = 300$ MHz (measured in iron-doped rutile at 85 GHz), an instantaneous bandwidth of 100 MHz results, which is well suited to investigation of interstellar spectral lines. The electronic gain is given by [5]

$$G_{\mathrm{dB}}{}^{e} = 27.3 \cdot S \cdot \frac{1}{|Q_m|} \cdot \frac{L}{\lambda_0}. \tag{2}$$

Here S = the slowing factor = c/v_g where c is the speed of light in vacuum and v_g is the group velocity with which the wave propagates through the maser structure, L is the length of active material from input to output, λ_0 = the free-space wavelength at the signal frequency, and Q_m is the magnetic quality factor of the maser material. In order to develop a useful traveling-wave millimeter-wave maser,

Manuscript received December 29, 1975; revised May 4, 1976. This work was supported by the National Science Foundation under Grants GP 26108, GP 38593X, and MPS75-09730. This paper is contribution number 227 of the Five College Radio Astronomy Observatory.

A. G. Cardiasmenos is with the Department of Physics and Astronomy and the Five College Radio Astronomy Observatory, University of Massachusetts, Amherst, MA 01002.
J. F. Shanley and K. S. Yngvesson are with the Department of Electrical and Computer Engineering and the Five College Radio Astronomy Observatory, University of Massachusetts, Amherst, MA 01002.

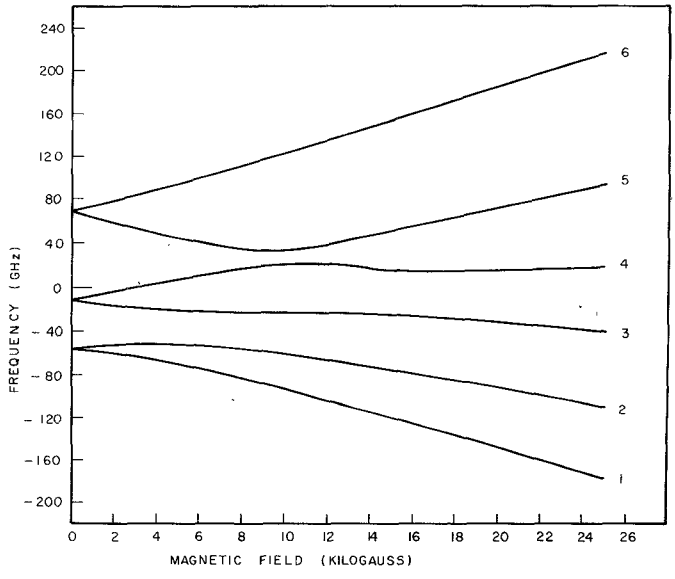

Fig. 1. Energy level diagram along a symmetry axis.

several design considerations must be taken into account. Among these are the following.

1) Choice of maser material and quantum electronic operating point useful at millimeter-wave frequencies.

2) Choice of microwave circuit based on dielectric and polarization properties of the maser material and desired tunable bandwidth.

3) Use of practical and relatively inexpensive pump sources providing sufficient power output to saturate the pump transition and thus give stable maser operation. This consideration presently is the one which determines the high-frequency limit of maser amplifiers.

4) Choice of a microwave circuit configuration which allows incorporation of a resonance isolator that can ensure stable unidirectional gain for the traveling-wave maser.

II. Active Maser Material

The active material used in this prototype millimeter-wave maser is iron-doped rutile (Fe^{3+}–TiO_2). This maser material has been used successfully in centimeter-wave maser amplifiers and a 13-mm traveling-wave maser amplifier [6] as well as for 3–4-mm wavelength cavity masers [1], [2], [4]. The wealth of information gathered in the development of these earlier masers made the use of iron-doped rutile the logical first choice for a millimeter-wave traveling-wave maser operational near 100 GHz. The energy level diagram for this material oriented with the external magnetic field along the a symmetry axis of the crystal is shown in Fig. 1.

The spin Hamiltonian of Fe^{3+}–TiO_2 which describes the six lowest spin states in a magnetic field is given by [7]

$$H = \frac{g\beta}{h}\boldsymbol{H}\cdot\boldsymbol{S} + D\left(S_z^2 - \frac{35}{12}\right) + E(S_x^2 - S_y^2) + \frac{a}{6}\left(S_x^4 + S_y^4 + S_z^4 - \frac{707}{16}\right) + \frac{7}{36}F\left(S_z^2 - \frac{75}{14}S_z^2 + \frac{81}{16}\right) \quad (3)$$

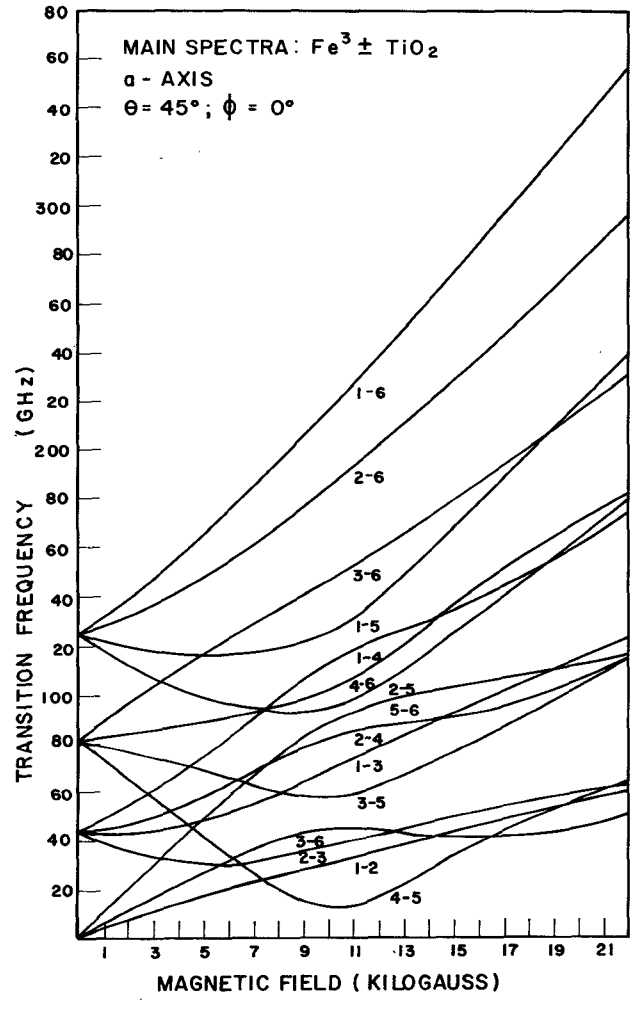

Fig. 2. Transition frequencies available along a axis for Fe^{3+}–TiO_2 as a function of applied magnetic field.

where the constants D, E, F, a, and g are measured as

$$D = 20.35 \text{ GHz}$$

$$E = 2.21 \text{ GHz}$$

$$F = -0.5 \text{ GHz}$$

$$a = 1.1 \text{ GHz}$$

$$g = 2.0.$$

The energy levels, transition frequencies, and transition matrix elements among the various levels as a function of the applied magnetic field, are found by diagonalizing the spin Hamiltonian matrix, which can be derived from (3). The diagonalization was accomplished numerically utilizing Jacobi's method on the UMass CDC CYBER 74 employing complex arithmetic directly on the 6 × 6 matrix, whereas previous calculations have developed a real 12 × 12 matrix and then diagonalized this. The direct diagonalization of the 6 × 6 matrix gives more accurate results, particularly for the eigenvectors, and thereby the transition probabilities.

In Fig. 2 we have plotted the transition frequencies as a function of applied magnetic field for the a-axis orientation.

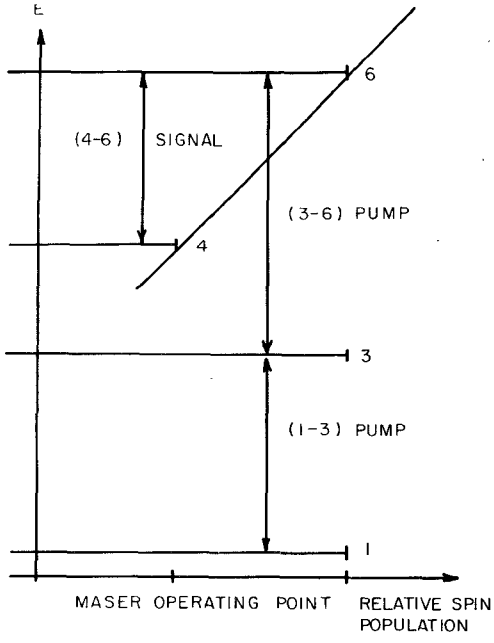

Fig. 3. 85–90-GHz maser operating point.

As can be seen, a large number of possible combinations of pump and signal frequency transitions may be used for maser operation. The two inequivalent sites available for the Fe^{3+} ion in the host lattice both contribute to the spin population for any given external magnetic-field intensity in this orientation, thus ensuring maximum gain.

Earlier Fe^{3+}–TiO_2 masers [1], [2] have utilized the so-called push–pull pumping scheme [5] in which two pump transitions are made to coincide in frequency by careful choice of the orientation of the magnetic field. This scheme allows good inversion while using only a moderately high pump frequency. The main disadvantage is that the orientation is very critical. Push–pull pumping is therefore not practical in Fe^{3+}–TiO_2, so much more so since traveling-wave masers use fairly long crystals and the crystal axes vary considerably in direction over typical crystal lengths. A better approach to maser operation over the 70–120 GHz frequency range involves the use of two relatively lower frequency pump sources, simultaneously pumping two transitions in order to produce an inversion of a third transition in the spin system. One such operating point, which we have successfully employed in this maser, involves the (1–3) transition with the magnetic field along the *a* axis [abbreviated *a*(1–3)] and the *a*(3–6) transition as the two pump transitions. These pumps invert the *a*(4–6) signal transition at 4 K and below. The operating point is illustrated in Fig. 3. For signal frequencies near 88 GHz, the *a*(1–3) pump frequency is 46–47 GHz while the *a*(3–6) pump must tune near 115 GHz. The nominal Fe^{3+} concentration in the crystals used is 0.035 percent by weight.

The use of iron-doped rutile is further complicated by its large anisotropic dielectric constant, which at liquid helium temperatures is approximately 256 parallel to the *c* axis and 150 in the perpendicular direction. Microwave losses due to the rutile host lattice are known to be insignificant at millimeter wavelengths.

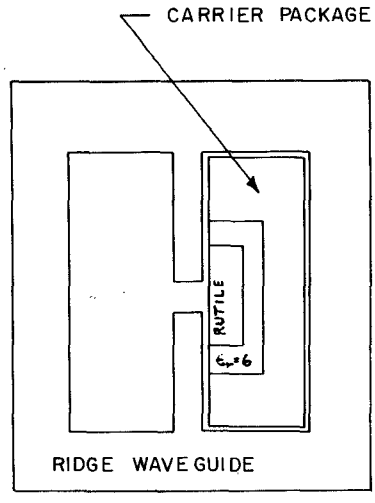

Fig. 4. Cross-sectional view through center of loaded maser structure.

III. Microwave Circuit

The microwave circuit for use with this maser must simultaneously propagate at three widely separated frequencies determined by the two pump frequencies of the operating point we have chosen. The large potential impedance mismatch between any normal waveguide transmission system and the fundamentally low-impedance system formed with the dielectric loading of the high-permittivity active material must be taken into consideration. Furthermore, since the gain of a traveling-wave maser is directly proportional to the slowing factor S [see (2)] of the electromagnetic wave propagating in the active medium, a large slowing is desired for efficient maser operation. All of these circuit characteristics have been incorporated into a new millimeter-wave transmission structure developed for use with this maser. It incorporates many of the characteristics of both ridge-guide and dielectric-image-guide transmission modes and is formed by the insertion of a metallic carrier package containing the rutile crystal into a slow-wave structure formed in the shape of a ridge waveguide with very thin ridges and narrow gap, a "fin line" [8]. As can be seen from the cross-sectional view of Fig. 4, the rutile crystal contained in its carrier package is centered on the slot which measures 0.1 mm in the prototype maser design. A standard tapered transition from the unloaded ridge-guide cross section to WR-42 waveguide cross section (0.356 × 1.067 cm) is extended from either end of the ridged section. The rutile crystal, having typical cross-sectional dimensions of 0.15 × 0.90 mm, is housed in a slot cut in the titanium metal carrier package. The slotted carrier package is then further lined with $\varepsilon_r = 6$ ceramic dielectric material. The $\varepsilon_r = 6$ liner and the rutile crystal are epoxied into place, and the entire package is ground and lapped flat for uniform contact with the ridge-guide surface. The choice of titanium metal for the carrier package was necessitated in order to match the thermal expansion coefficient of rutile, preventing serious thermally induced stresses from developing as the crystal package is cooled. The ridge-guide circuit is made of brass which has been gold plated and polished. A photograph of the maser structure appears in Fig. 5.

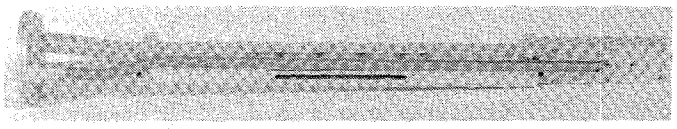

Fig. 5. Maser structure photograph.

Hexagonal ferrite materials, inserted in the carrier package along one side of the rutile cross section are utilized to produce unidirectional gain over the operational range of the maser. Special ferrite compositions[1] using aluminum substituted barium-iron oxides [12] exhibit the desired resonance field in the 80–95-GHz frequency range of this maser. These ferrite materials have measured resonance linewidths of several gigahertz, making them highly desirable for use as millimeter-wave maser resonance isolators. Because of the wide ferrite resonance linewidth, the rutile spin-resonance line is easily tracked over a wide range of frequencies with one ferrite material.

In order to understand the characteristics of the mode propagating in this system, two scaled models were constructed. Both the impedance and the dispersion relation were measured for various cross-sectional dimensions.

IV. Dispersion Relation

Dispersion curves were measured by the swept frequency resonance method, in which the resonances are observed for which the structure is $n\lambda_g/2$ long. The absolute number of wavelengths was then determined for several of the resonances by moving absorbing material along the structure so as to perturb the wave near the slot, while observing the power transmitted through the model. A frequency range from 1 to 18 GHz was covered in a model which was scaled by a factor of 7.5 from the 85–90-GHz maser structure dimensions. Coaxial cables were connected to the slot as input and output couplings. Since the outer walls of the ridge waveguide do not significantly affect propagation at frequencies well above cutoff, theoretical analysis modeled the ridge and the dielectric package in either a slot line or a low-order dielectric image-guide mode. In the first case, the ridges form the conventional conductors of a slot line while in the latter case, the ridges form the image plane of a lower order image-guide mode propagating almost entirely inside the rutile rod. Only image-guide modes without transverse currents across the slot are allowed due to the presence of the gap between the two ridges.

Dispersion relations for the slot-line case were obtained from Mariani *et al.* [9], [10]. In the case of the lower order image-guide modes, two coupled transcendental equations of the form

$$ak_x = \frac{m\pi}{2} - a\tan\left(\frac{k_x}{k_{x0}}\right) \tag{4}$$

$$bk_y = \frac{n\pi}{2} - a\tan\left(\frac{k_y}{k_{y0}}\right) \tag{5}$$

[1] Hexagonal ferrites were supplied by the Trans-tek Corporation, Gaithersburg, MD.

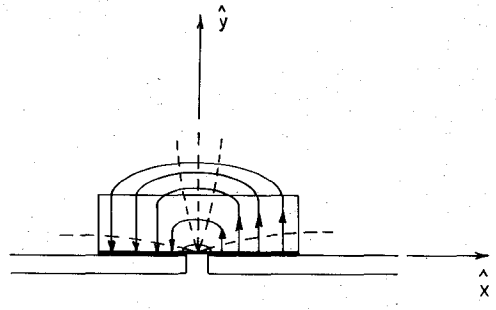

Fig. 6. Field configuration for E_y^{21} slot-fed image-guide mode. E: ——. H: – – –.

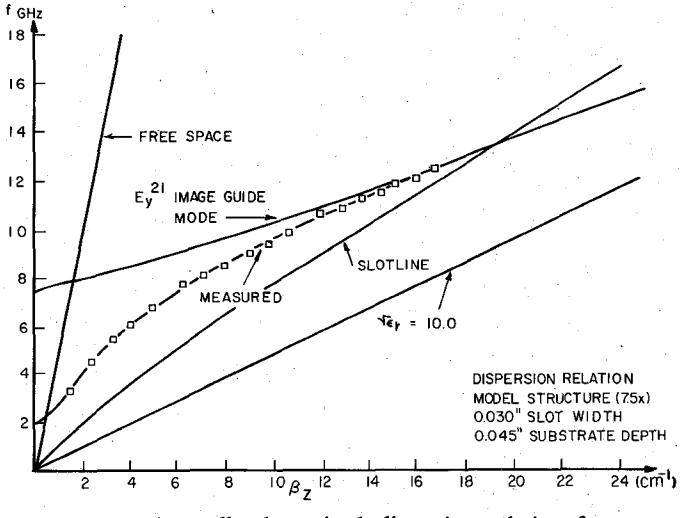

Fig. 7. Experimentally determined dispersion relation for maser structure.

where k_x,k_y are the transverse propagation constants in the image-guide medium, and were solved using the method of Knox and Toulios [11].

The lowest order E_y^{11} mode, although allowed in a normal image guide of these dimensions, does not couple to the field configuration of the unloaded slot due to its symmetry. The E_y^{21} mode, with the field configuration of Fig. 6, can easily couple to the unloaded ridge-guide fields (or to the field configuration of a typical slot-line mode) and we can appropriately characterize this mode as a slot-fed image-guide mode.

The measured dispersion relation is compared to slot-line and E_y^{21} image-guide modes in Fig. 7. It is evident that the measured curve tends asymptotically to the calculated E_y^{21} solution at frequencies high above cutoff. Note that no adjustable parameters are used in the theory. The cutoff frequency for the slot-fed mode is largely determined by the overall dimensions of the ridged waveguide walls. For long wavelengths (close to cutoff) the loaded structure wavelength is only minimally affected by the presence of the inhomogeneous dielectric loading of the rutile rod. The waveguide walls are closer to the slot than what is assumed in the ordinary slot-line mode theory, so the slot-line dispersion curve is not expected to fit the measured one in our case (see Fig. 7). A consistent qualitative

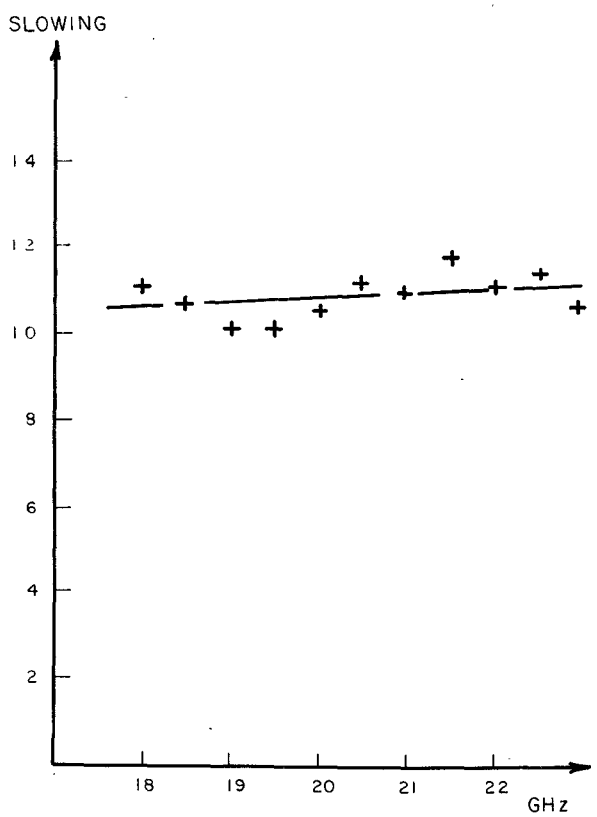

Fig. 8. Experimentally measured slowing (c/v_g) for 3.5X maser model structure.

description of the slot-fed image-guide mode can be obtained, however, if we assume a coupled mode system between the ridge-guide mode and the E_y^{21} image-guide mode. The coupling factor varies rapidly with frequency near the low β_z part of the E_y^{21} dispersion curve. It is well known that in this range the fields of the image guide rapidly spread outside the dielectric as the frequency decreases, explaining the rapid increase in coupling to the ridge-guide mode. Evidence for single-mode propagation in the model structure was reinforced by analyzing the characteristics of a miniature coaxial-cable-fed structure of the same type but with a scaling factor of 3.5. Measurements were made from 18–26 GHz in this case. We observed that the resonant transmission dips occurring as a function of frequency all conformed to points along the measured dispersion relation. No extraneous set of resonances with different guided wavelengths were observed. Thus one can confidently scale the dimensions and operating frequency range of the structure.

Using the well-known relation

$$S = \frac{c}{2\pi L \Delta f} \tag{6}$$

where Δf is the distance in hertz between resonances, and L is the physical length of the structure, we also found the slowing of the 3.5X model structure (see Fig. 8). It is interesting to note that the slowing approaches 13 for frequencies in the range of interest in developing this maser.

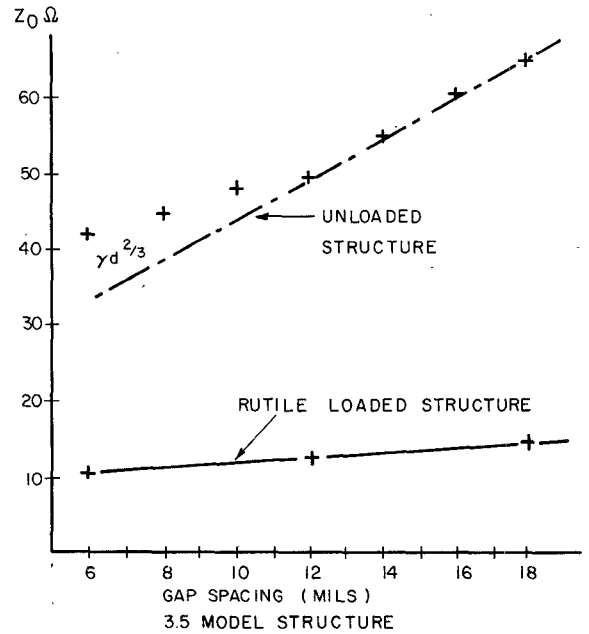

Fig. 9. Measured characteristic impedance in the 3.5X model structure.

The variation of slowing over the signal frequency range of the maser is remarkably small.

V. Characteristic Impedance

The 3.5X model structure was also used to measure the approximate loaded and unloaded impedance of the maser structure. Fifty-ohm semirigid coaxial cables were used to feed signals to and from the model. The return loss of the model structure, measured as a function of gap spacing and/or dielectric loading, determined the VSWR and therefore the impedance relative to 50 Ω for the structure. The loaded and unloaded impedance of the structure plotted in Fig. 9 indicates that an impedance ratio of approximately 4 to 1 exists between the unloaded ridge and the slot-fed image-guide mode. The measured impedance of the fin-line section agrees with the $\gamma d^{2/3}$ dependence cited by Robertson [8] for a similar geometry utilized at lower frequencies. The significant reduction in impedance variation as a function of ε_r for large values of permittivity is another advantage of the slot-fed image-guide mode.

The structure can be matched over a wide frequency range using a quarter-wave transformer approach. Impedance measurements made on the carrier package cross section without the presence of the rutile crystal, but containing the $\varepsilon_r = 6$ ceramic material, indicate an impedance level nearly that of the geometric mean impedance required for conventional quarter-wave transformer operation.

VI. 85–90-GHz Maser Operation

A series of carrier packages were prepared for the 85–90-GHz maser structure, with relevant parameters scaled directly from the model structure cross section. The loaded maser structure was mounted in a newly developed superconducting magnet and experiments were conducted at 4 and 2 K in a batch-cooled liquid-helium dewar. Both pump

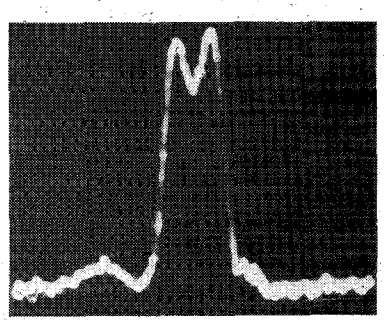

Fig. 10. Maser swept frequency response. 15-dB electronic gain/50-MHz bandwidth at a center frequency of 87.4 GHz.

frequencies enter the maser through a multiplexer in the signal output waveguide, since no separate pump waveguide is used in this design. All signals enter and exit the maser through oversized WR-42 waveguides, used to reduce the waveguide loss contributions. The matched maser carrier package has a measured maximum VSWR referred to the crystal carrier package interface of 1.65 between 85 and 95 GHz. The bandwidth of the quarter-wave transformer utilized, although not yet measured, can be approximately determined from 75 to 95-GHz swept measurements to be greater than 50 GHz. Consistent with this, the transformer was found to greatly improve pump saturation for the 115-GHz pump. The 43-GHz pump transition, although not matched to the crystal package in this prototype design, saturates easily due to the strong pump transition matrix element involved.

Electronic gain of 3–5 dB with bandwidths of 140 MHz have been obtained using short-length (0.7-cm) prototype packages. Presently, experiments are being conducted to lengthen this prototype amplifier to produce 15–20-dB net gain, usable for radio astronomy applications. A total length of 7.0 cm is available in the maser structure for accommodation of the active material.

Pump saturation for both pump transitions is excellent—a reduction of 3 dB in pump power producing less than 0.25-dB change in the overall amplifier gain for either pump transition.

Recent experiments, where the $a(4–5)$ transition was pumped in addition to the $a(1–3)$ and $a(3–6)$ pump transitions, produced electronic gain of 15 dB in a similar short-length package. It was found that the addition of this third pump transition increased the inversion ratio from 1.1 to 2.3. A typical amplifier response curve at a center frequency of 87.4 GHz is illustrated in Fig. 10. Use of an extended interaction oscillator, or a swept IMPATT oscillator as a pump source for the $a(3–6)$ transition, allowing a frequency sweep of ± 200 MHz around the center frequency of the pump transition, would produce similar gain over a much wider bandwidth. Experiments along these lines are planned in the near future. An eventual goal of 20-dB net gain and 200-MHz bandwidth seems quite feasible for this design.

VII. Conclusion

We have demonstrated the feasibility of low-noise traveling-wave maser amplifiers at millimeter wavelengths. Use of these amplifiers will greatly increase the sensitivity limit of radioastronomical research in the 70–120-GHz frequency range. The waveguide circuit employed is neither critical nor difficult to manufacture, and serves well as the control over the mode purity over this entire range of frequencies, allowing tunable bandwidth of the maser of about a standard waveguide band. The operating frequency of the maser structure, developed around the nonresonant slowing of the slot-fed image-guide mode, is easily modified through direct geometrical scaling. We hope to utilize this maser receiver on the new 13.7-m FCRAO precision millimeter-wave telescope in the fall of 1976.

Acknowledgment

The authors wish to thank T. Kozul of Baytron Microwave Corporation for his support, and P. Crandell and J. Kuno of Hughes Electron Dynamics Division and R. West of the Trans-Tek Corporation for their help which has been invaluable to the development of the maser prototype. They also wish to thank Prof. G. R. Huguenin for his support and unfailing inspiration.

References

[1] D. L. Carter, *JAP*, vol. 32, p. 2541, 1961.
[2] A. Mole and M. Soutif, *L'Onde Electrique*, vol. 47, p. 183, 1967.
[3] I. I. Eru, S. A. Peskovatskiy, and A. N. Charnets, *IEEE J. Quantum Electr.*, vol. QE-4, p. 723, 1968.
[4] W. E. Hughes, *Proc. IRE*, vol. 50, p. 1691, 1962.
[5] A. E. Siegman, *Microwave Solid State Masers*. New York: McGraw-Hill, 1964.
[6] K. S. Yngvesson, A. G. Cardiasmenos, and E. L. Kollberg, IEEE Intern. Microw. Symp., Boulder, Colorado, June 1973.
[7] D. L. Carter and A. Okaya, *Phys. Rev.*, vol. 118, p. 1485, 1960.
[8] S. D. Robertson, *IRE Trans. Microwave Theory Tech.*, vol. MTT-6, p. 263, 1956.
[9] E. A. Mariani, private communication.
[10] E. A. Mariani, C. P. Heinzman, J. P. Agrios, and S. B. Cohn, *IEEE Trans. Microwave Theory Tech.*, vol. MTT-17, p. 109, 1969.
[11] R. M. Knox and P. P. Toulios, *Proc. of the Symposium on Submillimeter Waves*. Polytechnic Press, 1970, pp. 497–516.
[12] D. J. De Bitetto *et al.*, *Proc. of the Symposium on Millimeter Waves*. Polytechnic Press, 1960, pp. 95–108.